*Int. J. Electrochem. Sci.*, 15 **(2020)** 10825 – 10843, doi: 10.20964/2020.11.51

**International Journal of**
**ELECTROCHEMICAL**
**SCIENCE**
www.electrochemsci.org

# Study on Iron Sulphide Inhibition and Corrosion of 80S and 110SS steels in Acid Solutions Containing $H_2S$ and $CO_2$

*Z.F. Yin*[1,2,*], *L. Liu*[1,2], *Y. Wang*[1], *T.Q. Yang*[3], *Y.X. Chen*[4]

[1] School of Mechanical and Material Engineering, Xi'an University, Xi'an 710065, P R China
[2] Shaanxi Key Laboratory of Surface Engineering and Remanufacturing, Xi'an 710065, P R China
[3] Research Institute of Shaanxi Yanchang Petroleum， (Group) Co. LTD, Xi'an 710065, P R China
[4] Yanchang Petroleum Group Exploration Company, Yan'an 716000, P R China
*E-mail: yinzhifu919@sohu.com

*Received:* 10 July 2020 / *Accepted:* 31 August 2020 / *Published:* 30 September 2020

---

Corrosion behavior and characteristics of 80S and 110SS steels were investigated in acid solutions containing $H_2S$ and $CO_2$ at 45°C by the potentiodynamic polarization sweep, EIS and SEM with EDX. The EIS data fitted by ZsimpWin software were theoretically analyzed and discussed. The results indicated that the corrosion potential became more negative and that the corrosion current density decreased as the $Na_2S{\cdot}9H_2O$ concentration increases from 0 to 2.0*wt*.%, with the obvious reverse sweep characteristics occurring in anodic polarization branch curve in 2.0*wt*.% $Na_2S{\cdot}9H_2O$ case. Warburg impedance characteristics of diffusion process in a low frequency region following a depressed capacitive semi-circle in the intermediate frequency region was observed on 110SS steel with the addition of certain $Na_2S{\cdot}9H_2O$ concentration. The phase angle peaks for $H_2S$ containing cases in the intermediate frequency region shifted to a low frequency direction and rised toward -90° significantly. The amounts of S element in the "first deposition" corrosion product layer were higher than those in the "second deposition" corrosion product crystals. One corrosion model related to $H_2S$ and $CO_2$ corrosion was proposed.

---

**Keywords:** 80S and 110SS steels; $H_2S/CO_2$ corrosion; Polarization curve; EIS; Corrosion product layer; Corrosion model

## 1. INTRODUCTION

Corrosion of metallic materials occurred internally and externally when tubing, casing and pipeline steels were used in oil and gas production environments containing $H_2S$ and $CO_2$ aggressive gases, leading to costly repairs, shutdowns, as well as health and environmental hazards due to corrosion failure, which were the most intractable problems in recent decades [1,2]. Corrosion behavior of metallic materials in the $H_2S$ and $CO_2$ containing environment was influenced by many important factors such as temperature, $H_2S$ and $CO_2$ partial pressures, fluid velocity, corrosion product, water percent, chemical composition of produced fluid and material organization. Although carbon steels possessed the acceptable mechanical properties and low-cost in oil and gas production industry, they were very susceptible to sweet corrosion and sour ($CO_2$+$H_2S$) corrosion [3-5].

he intermediate product $FeHS^+_{ads}$ could produce and adsorbed on the local steel surface, and then caused the formation of mackinawite ($FeS_{1-x}$). Meanwhile, amorphous $FeCO_3$ could also directly form on the local steel surface. The corrosion products are composed of $Fe(OH)_2$, $FeCO_3$ and $FeS_{1-x}$ according to the solid state reaction mechanism and/or the precipitation mechanism in $H_2S/CO_2$ containing environments. The corrosion product layer growth depends primarily on the kinetics of the layer formation. In contrast to the relatively iron carbonate precipitation in pure $CO_2$ corrosion environment, in $H_2S$-containing environment, lots of types of iron sulfides may form, such as ferrous sulfide, mackinawite, cubic ferrous sulfide, greigite, pyrrhotite, troilite and pyrite [6].

In the $CO_2$-$H_2S$-$H_2O$ corrosion system, lots of open studies regarded the direct hydration of $H_2S$ to be the dominant cathodic reaction, the dominant cathodic reaction might be the reduction of $H^+$ and $H_2S$ played a buffering role in the mechanism [6-8]. It was also well proposed that $H_2S$ played a dual role in $CO_2$ corrosion system, while in trace amounts the instantaneous formation of FeS layer decreased corrosion rate (inhibition effect), higher concentration increases the rate of corrosion (acceleration effect) [9,10]. $H_2S$ presented an acceleration effect to both the anodic iron dissolution and the cathodic hydrogen evolution except for certain special condition where the lower $H_2S$ concentration and the longer immersion time were met simultaneously [11,12]. The inhibition characterization could be found, which was related to the formation of pyrite, troilite and mackinawite. Masamura *et al.* [13] also proposed that the intermediate product of $FeSH^+_{ad}$ can dissolve into ferrous ion or form rich-iron compounds $FeS_{1-x}$.

Based on some researches on corrosion behavior and mechanism in $H_2S$ containing brines by EIS method, there were one capacitive loops or an inductive loop appeared at low frequency due to an adsorbed intermediate related to sulphide formation [14]. Arzola *et al.* [15] performed tests in 30 g/L NaCl solutions with various $H_2S$ concentrations ranging from 100 mass ppm to 2550 mass ppm, it was shown that the impedance results of impedance plots were quite different from those obtained by previous authors. They consisted of a capacitive loop at high frequency interpreted by the charge transfer resistance followed by a 45$^o$ tail at low frequency representing a diffusion process.

Although research work of $H_2S/CO_2$ corrosion in the past several decades was conducted by corrosion engineers, the literatures were somewhat confusing and often seemingly inconsistent. Iron sulfide chemistry was very complex and seemingly minor changes in test conditions can often lead to dramatically different results. The common method to evaluate metallic materials subjecting to corrosion under condition of stress was carried out in NACE TM 0177 solution ($CH_3COOH$, $CH_3COONa$, NaCl, pH 3.5, with and without the saturation of $H_2S$) [16]. However, rarely available literatures about the corrosion mechanism of carbon steel were discussed in the presence of HAc, chlorides, $CO_2$ and $H_2S$ [17,18]. In addition, the researches of $H_2S/CO_2$ corrosion were focused on low carbon steel, little on anti-sulfur steels. The present work was to conduct a comparative study on the corrosion behavior between 80s steel and 110SS steel by the methods of potentiodynamic polarization sweep, electrochemical impedance spectroscopy (EIS) and scanning electron microscopy (SEM) with energy dispersive x-ray (EDX) in the solutions containing 3.5*wt.*%NaCl and 0.5*wt.*%$CH_3COONa$ with the addition of various concentrations of $Na_2S\cdot 9H_2O$ and saturated $CO_2$ at 45°C, where $Na_2S\cdot 9H_2O$ could turn into $H_2S/HS^-$ species in the acid solution.

## 2. EXPERIMENTAL METHOD

### *2.1. Specimen and solution preparation*

All specimens were machined from 80S and 110SS steels with the chemical composition (*wt*.%) were shown in Table 1. The specimen (the working electrode) was a cylindrical geometry, 10.0 cm in diameter and 3.0 cm in height, embedded in epoxy resin with an exposed working area of 0.785 $cm^2$. A new specimen was always used for each experiment and prior to the electrochemical tests the working surfaces were wet-ground with SiC sand papers up to 1200 grit, then rinsed with alcohol and triply with deionized water.

**Table 1.** Chemical compositions of specimens of 80S and 110SS steels

| Material | Element contents（*wt*.%） | | | | | | | |
|---|---|---|---|---|---|---|---|---|
| | C | Si | Mn | P | S | Cr | Ni | Mo |
| 80S | 0.23 | 0.19 | 0.46 | 0.006 | 0.002 | 0.91 | 0.03 | 0.27 |
| 110SS | 0.20 | 0.24 | 0.49 | 0.007 | 0.002 | 0.50 | 0.02 | 0.78 |

Analytical grade reagents were used as 3.5*wt*.%NaCl, 0.5*wt*.%$CH_3COONa$, and 1 L deionized water to prepare the experimental base solution. The base solution was introduced by the different concentrations of 0.1*wt*.%, 0.5*wt*.%, 1.0*wt*.%, 2.0*wt*.% $Na_2S\cdot 9H_2O$ since it would turn into $H_2S/HS^-$ in acidic solution and saturated $CO_2$ in order to simulate the gas field acid corrosion environments containing $H_2S$ and $CO_2$. In addition, $CH_3COONa$ could also turn into $CH_3COOH/CH_3COO^-$. The electrolyte solutions were deaerated by purged with nitrogen with $CO_2$ respectively bubbling for 30 min prior to the experiments. The $CO_2$ bubbles successively were through the solutions in the electrochemical measurements.

### *2.2. Electrochemical measurement*

The electrochemical tests were conducted by potentiodynamic polarization sweep and electrochemical impedance spectroscopy (EIS) methods in a conventional three electrode cell of Ametek Princeton PARSTAT 4000A+. The counter electrode was a pair of graphites, the reference electrode was a saturated calomel electrode (SCE) and 80S and 110SS specimens acted as the working electrode. The polarization curves were measured by sweeping the potential from -0.25 V vs. open circuit potential (OCP) to 0.25 V vs. SCE at a scan rate of 0.25 mV/s.

The EIS measurements were carried out at OCP by applying sinusoidal amplitude perturbation of 10 mV at a frequency from 100 kHz to 10 mHz. All potentials were measured with respect to SCE. Each experiment was conducted at least two times for better reproducibility. The ZsimpWin software was used to analyze the EIS experimental data by equivalent circuit models. All experimental temperature was controlled at 45°C.

### *2.3. Corrosion product layer analysis*

The surface morphology and chemical composition of corrosion product layers on specimens were characterized using the JSM-6610LV scanning electron microscopy (SEM) equipped with energy dispersive X-ray (EDX).

## 3. RESULTS AND DISCUSSION

### *3.1. Potentiodynamic polarization curves*

#### *3.1.1. Measurement on 80S steel*

Figure 1 shows the corrosion behavior on the potentiodynamic polarization curves on 80S steel in $CO_2$-containing base solution with different concentrations of 0, 0.1*wt*.%, 0.5*wt*.%, 1.0*wt*.%, 2.0*wt*.% $Na_2S\cdot 9H_2O$ at 45°C. The cathodic branch curves shifts to the left direction(*i.e.*, the current density decreasing direction) with the increase of $Na_2S\cdot 9H_2O$ (*i.e.*, $H_2S/HS^-$) concentration. It shows one limiting cathodic current region in the cathodic branch curve for $H_2S$-free case (curve 1), involving the diffusion limited current of $H^+$ reduction, and chemical reaction controlled current of $H_2CO_3$ reduction and $CH_3COOH$ reduction. For 0.1*wt*.% $Na_2S\cdot 9H_2O$ case (curve 2), the similar limiting cathodic current region can be seen in the cathodic branch, besides the effect of $H^+$, $H_2CO_3$, $CH_3COOH$ reductions, involving also the additional slight effect of $H_2S$ reduction. However, for the increased $Na_2S\cdot 9H_2O$ cases (curves 3-5), the mass transfer limiting cathodic current plateau is not observed. At the more negative potential in the cathodic branch curves, only very weak charge transfer impact characteristics by direction $H_2O$ reduction as compared to the characteristics of both curve 1 and curve 2. The anodic branches of polarization curves except for curve 5 in Fig. 1 have similar characteristics regardless of the different concentrations of $H_2S/HS^-$, and only a small turning peak is observed around -0.7 V of the anodic branches of polarization curve 3 and curve 4, which is probably related to the instantaneous adsorption of $OH^-_{(aq)}$, $HCO_3^-{}_{(aq)}$, $CH_3COO^-_{(aq)}$ and $HS^-_{(aq)}$ forming intermediates with steel substrate. For the 2.0*wt*.% $Na_2S\cdot 9H_2O$ case, it can be easily seen that the current density decreases obviously when the sweep potential from -0.71 V to -0.61 V and then the current density increases continuously in the anodic branch of polarization curve 5, which is attributed to the firstly formed protective corrosion product layers against further corrosion and then the breakdown of protective corrosion layers causing increased corrosion again. In addition, it is worth noting that the polarization tail region of anodic curve 5 beyond -0.5 V significantly shifts in the positive direction of potential, meaning that the current density largely decreases due to the deposition of corrosion products and the formation of protective layers corresponding to the sulfide-related reactions.

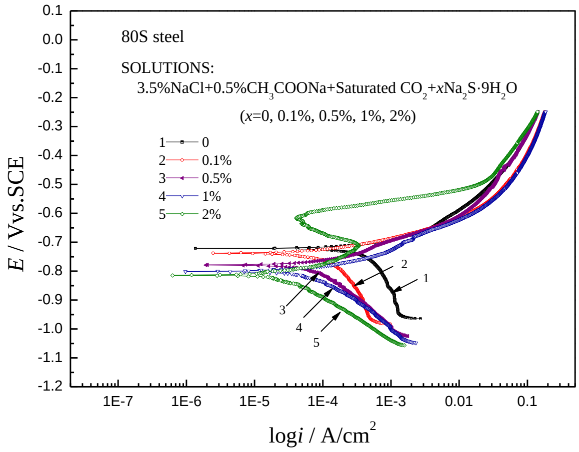

**Figure 1.** Effect of $H_2S$ on polarization curves of 80S steel at 45°C in acidic solutions containing $H_2S$ and $CO_2$

The corrosion parameters corresponding to the potentiodynamic polarization curves of 80S steel are listed in Table 2. It is seen that the corrosion potential ($E_{corr}$) of 80S steel becomes more negative (-721.2 mV to -811.0 mV vs.SCE) as the $Na_2S·9H_2O$ concentration increases (from 0 to 2.0*wt*.%). The corrosion current density ($i_{corr}$) of anti-sulfur steel 80Sdecreases with an increase in $Na_2S·9H_2O$ concentration (*i.e.*, $H_2S/HS^-$). It indicates that $H_2S$ can lead to the retardation effect on $H_2S/CO_2$ corrosion of carbon steel, which is in agreement with the results from research by Choi, *et al.* [19] and Veloz, *et al.* [20], while disagrees with the results by Tang, *et al.* [21] and Ma *et al.* [22]. Because $HS^-$ can be strongly chemisorbed on steel surface and displace adsorbed $OH^-$, it slows down dissolution rate of carbon steel. Compared with the $H_2S$-free case, the anodic Tafel slopes ($\beta_a$) of 80S steel have small differences in mixed $H_2S/CO_2$ solution containing different $H_2S/HS^-$, which indicates that the concentrations of $H_2S/HS^-$ contributed similarly to the anodic dissolution process. However, the cathodic Tafel slope ($\beta_c$) of 80S steel in Table 2 is considerably dependent on the $H_2S/HS^-$ concentrations. This fact is that greater values of these $\beta_c$ values are compared with those $\beta_a$ values, indicating that the complex nature of the corrosion processes is mainly controlled by cathodic reactions.

**Table 2.** Corrosion parameters of the polarization curves of 80S steel at 45°C in acidic solutions containing $H_2S$ and $CO_2$

| $Na_2S·9H_2O$ /wt.% | $E_{corr}/mV$ | $i_{corr}/\mu A·cm^{-2}$ | $\beta_a/mV·dec^{-1}$ | $\beta_c/mV·dec^{-1}$ |
|---|---|---|---|---|
| 0 | -721 | 589.4 | 75 | -644 |
| 0.1 | -739 | 137.1 | 59 | -343 |
| 0.5 | -779 | 103.9 | 82 | -227 |
| 1.0 | -800 | 79.5 | 66 | -174 |
| 2.0 | -811 | 34.6 | 78 | -160 |

### *3.1.2. Measurement on 110SS steel*

The corrosion behavior of the potentiodynamic polarization curves on 110SS steel in $CO_2$-

containing base solution with different concentrations of 0, 0.1*wt.*%, 0.5*wt.*%, 1.0*wt.*%, 2.0*wt.*% $Na_2S\cdot9H_2O$ at 45°C are shown in Fig. 2.

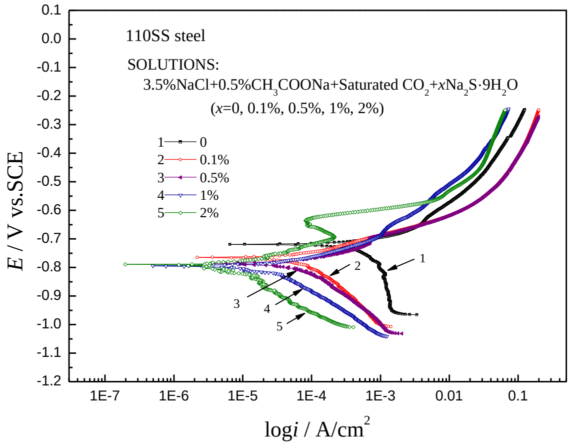

**Figure 2.** Effect of $H_2S$ on polarization curves of 110SS steel at 45°C in acidic solutions containing $H_2S$ and $CO_2$

It can be seen that the similar corrosion characteristics of 110SS in the cathodic branch curves and the anodic branch curves for the corresponding concentrations of introduced $Na_2S\cdot9H_2O$ chemical agent are observed as compared to the characteristics of 80S. There are some small differences between the characteristics of polarization curves with respect to the same solution condition at 45°C. For instnce, the limiting cathodic current region can not be observed on 110SS for 0.1*wt.*% $Na_2S\cdot9H_2O$ case in the cathodic branch (curve 2) in Fig. 2, just opposite result on 80S in Fig. 1. In addition, compared with curve 5 in Fig.1, there is one conspicuous narrow of the anodic polarization branch curve 5 in reverse sweeping region in Fig. 2, indicating that 110SS steel has less sensitive compared with 80S steel with the effect of $H_2S/HS^-$ species.

**Table 3.** Corrosion parameters of the polarization curves of 110SS steel at 45°C in acidic solutions containing $H_2S$ and $CO_2$

| $Na_2S\cdot9H_2O$ /wt.% | $E_{corr}$/mV | $i_{corr}$/μA·cm$^{-2}$ | $\beta_a$/mV·dec$^{-1}$ | $\beta_c$/mV·dec$^{-1}$ |
|---|---|---|---|---|
| 0 | -719 | 755.4 | 68 | -614 |
| 0.1 | -766 | 93.3 | 76 | -225 |
| 0.5 | -786 | 82.3 | 68 | -196 |
| 1.0 | -800 | 28.6 | 66 | -151 |
| 2.0 | 789 | 6.4 | 56 | -147 |

In Table 3, the corrosion parameters corresponding to the polarization curves of 110SS steel at 45°C in acidic solutions containing $H_2S$ and $CO_2$ can provide more information about the overall corrosion process. The $E_{corr}$ values of 110SS steel becomes more negative with the increase of $Na_2S\cdot9H_2O$ concentration (*i.e.* $H_2S/HS^-$) except for 2.0*wt.*% $Na_2S\cdot9H_2O$ case, but there are obvious differences between the $E_{corr}$ values of 110SS and 80S steels. The $i_{corr}$ values of 110SS steel decrease with increasing $Na_2S\cdot9H_2O$ concentration, indicating the corrosion rate decreases with the retardation effect of $H_2S/HS^-$ species. As compared to the $i_{corr}$ values of 80S steel in Table 2, the corresponding $i_{corr}$ value of 110SS steel in Table 3 decreases at same solution condition, which indicates that 110SS steel has stronger resistance than 80S steel in the $H_2S$ containing environment.

It can be seen that the main compositional differences between 80S and 110SS steels are in the Cr and Mo contents as shown in Table 1, and roughly the same Ni and Mn contents. Generally, Mn combined with S can form the inclusion of MnS, which serves as microcathode in steel and promotes local corrosion which plays a negative role in $H_2S/CO_2$ corrosion. The little quantity of Ni element has almost little effect on the corrosion resistance. In Table 1, the content of alloy element Cr in 80S steel is much more than that in 110SS steel, *i.e.* 80S (0.91%) and 110SS (0.50%), but alloy element Mo in 80S steel (0.27%) is much smaller amounts than that in 110SS steel (0.78%). According to the data of corrosion current densities of polarization curves, 110SS steel has stronger resistance than 80S steel probably due to Mo has one important effect on $H_2S/CO_2$ corrosion under the condition of a certain range of Cr and Mo synergy.

## *3.2. Electrochemical impedance spectroscopy*

### *3.2.1. Measurement on 80S steel*

Electrochemical impedance spectroscopy (EIS) as a transient electrochemical technique is often applied for it only has a slightly disturbance to corrosion process. The Nyquist plots and Bode plots of 80S steel obtained in $CO_2$-containing base solution with different concentrations of 0, 0.1*wt.*%, 0.5*wt.*%, 1.0*wt.*%, 2.0*wt.*% $Na_2S\cdot9H_2O$ at 45°C are respectively presented in Fig. 3 and Fig. 4. The testing results are shown in Fig. 3a and Fig. 4a, with good fitting results by equivalent circuit models of ZsimpWin software are shown in Fig. 3b and Fig. 4b. The Nyquist plots of 80S steel demonstrate that the shape and size have obvious differences for different $H_2S/HS^-$ concentrations. For the $H_2S$-free case, the Nyquist plot has three times constants consisting of one depressed capacitive semicircle in the intermediate frequency region, an inductive small reactance semicircle and a small capacitive semicircle at the low frequency region. For the addition of $Na_2S\cdot9H_2O$, the corrosion behavior of Nyquist plot has only one time constant, *i.e.*, the inductive reactance semicircle and the capacitive semicircle in the low frequency region disappear due to the active areas of steel surface completely occupied by corrosion products.

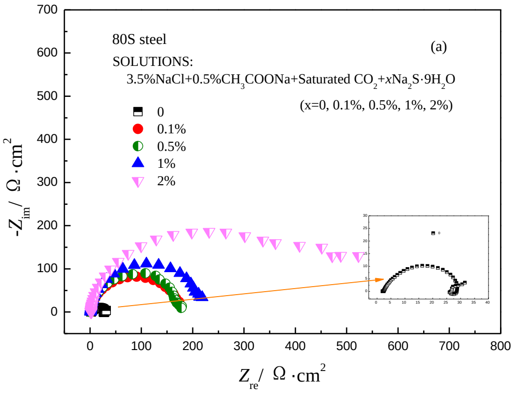

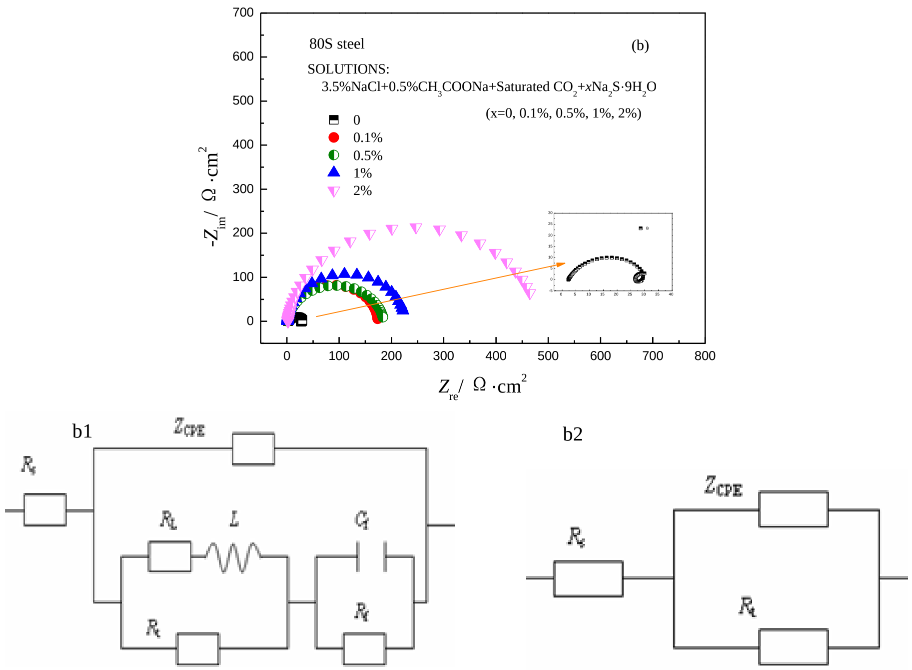

**Figure 3.** Effect of $H_2S$ on Nyquist plots of 80S steel at 45°C in acidic solutions containing $H_2S$ and $CO_2$. (a) testing curves; (b) fitting curves and equivalent current models

The depressed capacitive semi-circles are probably attributed to the influence of the heterogeneous surface roughness, the non-uniform distribution of current density and presence of corrosion product film on metal surface [23]. It is clearly observed that the diameter of the capacitive semicircle increases with the increase of $H_2S/HS^-$ concentrations in the intermediate frequency region. Moreover, the diameters of the capacitive semicircles have small differences in 0.1*wt.*%, 0.5*wt.*%, 1.0*wt.*% $Na_2S\cdot9H_2O$ cases, whereas the diameter is much larger for the 2.0*wt.*% $Na_2S\cdot9H_2O$ case than others.

The corresponding Bode plots in Fig. 4 show that, compared with $H_2S$-free case, the phase angle peaks for $H_2S$-containg cases at the intermediate frequency region shift to the left direction (low frequency direction) and rises toward -90° significantly, which is mainly induced by the formation of the corrosion film on the surface of electrode [24]. The maximum phase angles dramatically increase from about -43° in $H_2S$-free condition to about -72° ~ -80° in the $H_2S$-containing conditions, suggesting that the double layer capacitances in the sour corrosion are more ideal than the one in the $H_2S$-free condition. An increase in capacitance will require longer charging, which then will shift the phase angle peak to be at a lower frequency (*i.e.*, left direction). However, the phase angle peaks for different $H_2S$-containing cases at 45°C have minor differences in the intermediate frequency region.

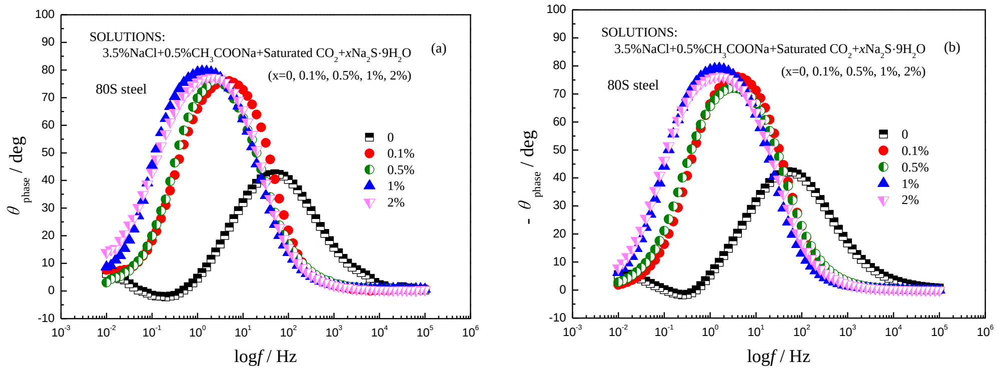

**Figure 4.** Effect of $H_2S$ on Bode plots of 80S steel at 45°C in acidic solutions containing $H_2S$ and $CO_2$. (a) testing curves; (b) fitting curves

The fitting parameters of impedance data of 80S steel obtained at 45°C by ZsimpWin software are shown in Table 4, and the corresponding equivalent circuit models are shown in Fig. 3b$_1$ to Fig. 3b$_2$. For these circuit models, $R_s$ is the solution resistance between the working and reference electrodes, $R_t$ is the charge transfer resistance, $L$ is the inductance related with the adsorption products, $R_L$ is the inductive resistance of adsorption products, $C_f$ is the capacitance, and $R_f$ is the resistance of corrosion product layer, respectively. In general, the constant phase element (CPE) represents the impedance of the capacitance element Q, which is widely used as scattered circuit element in equivalent circuits when non-ideal frequency response is present.

**Table 4.** Fitting parameters from the Nyquist plots of 80S steel by equivalent circuit models at 45°C in acidic solutions containing $H_2S$ and $CO_2$

| Parameters | $x$ Na$_2$S·9H$_2$O | | | | |
|---|---|---|---|---|---|
| | 0 | 0.1% | 0.5% | 1% | 2% |
| $R_s$ ($\Omega\cdot cm^2$) | 2.2 | 1.6 | 1.7 | 1.1 | 2.0 |
| $Q$-$Y_0$ ($\Omega^{-1}\cdot cm^{-2}\cdot s^n$) | $1.7\times10^{-3}$ | $2.8\times10^{-3}$ | $3.5\times10^{-3}$ | $7.1\times10^{-3}$ | $3.9\times10^{-3}$ |
| $Q$-$n$ | 0.74 | 0.97 | 0.92 | 0.97 | 0.93 |
| $R_t$ ($\Omega\cdot cm^2$) | 30.2 | 172.7 | 183.7 | 224.9 | 497.1 |
| L ($H\cdot cm^2$) | 56.9 | - | - | - | - |
| $R_L$ ($\Omega\cdot cm^2$) | 121.9 | - | - | - | - |
| $C_f$ ($F\cdot cm^{-2}$) | 2.1 | - | - | - | - |
| $R_f$ ($\Omega\cdot cm^2$) | 5.9 | - | - | - | - |

In Table 4, at 45°C, the $R_t$ value of 80S steel remarkably increases with the $Na_2S\cdot9H_2O$ concentration from 0.1*wt.*% to 2.0*wt.*%, which indicates that the corrosion resistance of 80S steel increases with $H_2S/HS^-$ concentration increasing. The result is accordant with the result from polarization curves above. $Q$-$n$ is around 0.9 in each solution containing $H_2S/HS^-$, suggesting the non-ideality of double layer capacitor between steel surface and solution. This was caused by the non-homogeneity of the double layer due to the formation of corrosion products. The CPE has also been referred to as the film capacitance on the surface related to the transport of ions/vacancies through the lattice structure of the corrosion product film [25].

### *3.2.2. Measurement on 110SS steel*

The Nyquist plots of 110SS steel obtained in $CO_2$-containing base solution with different concentrations of 0, 0.1*wt*.%, 0.5*wt*.%, 1.0*wt*.%, 2.0*wt*.% $Na_2S{\cdot}9H_2O$ at 45°C are presented in Fig. 5. For the $H_2S$-free case, the Nyquist plot of 110SS steel consists of three time constants, *i.e.*, one depressed capacitive semicircle at the intermediate frequency region, an inductive reactance semicircle and a small capacitive semicircle in the low frequency region at 45°C, which is similar to the corrosion characteristics of 80S steel. It shows the co-effects of both adsorption of $CO_{2(aq)}$ molecules and deposition of corrosion product layers on metal surface.

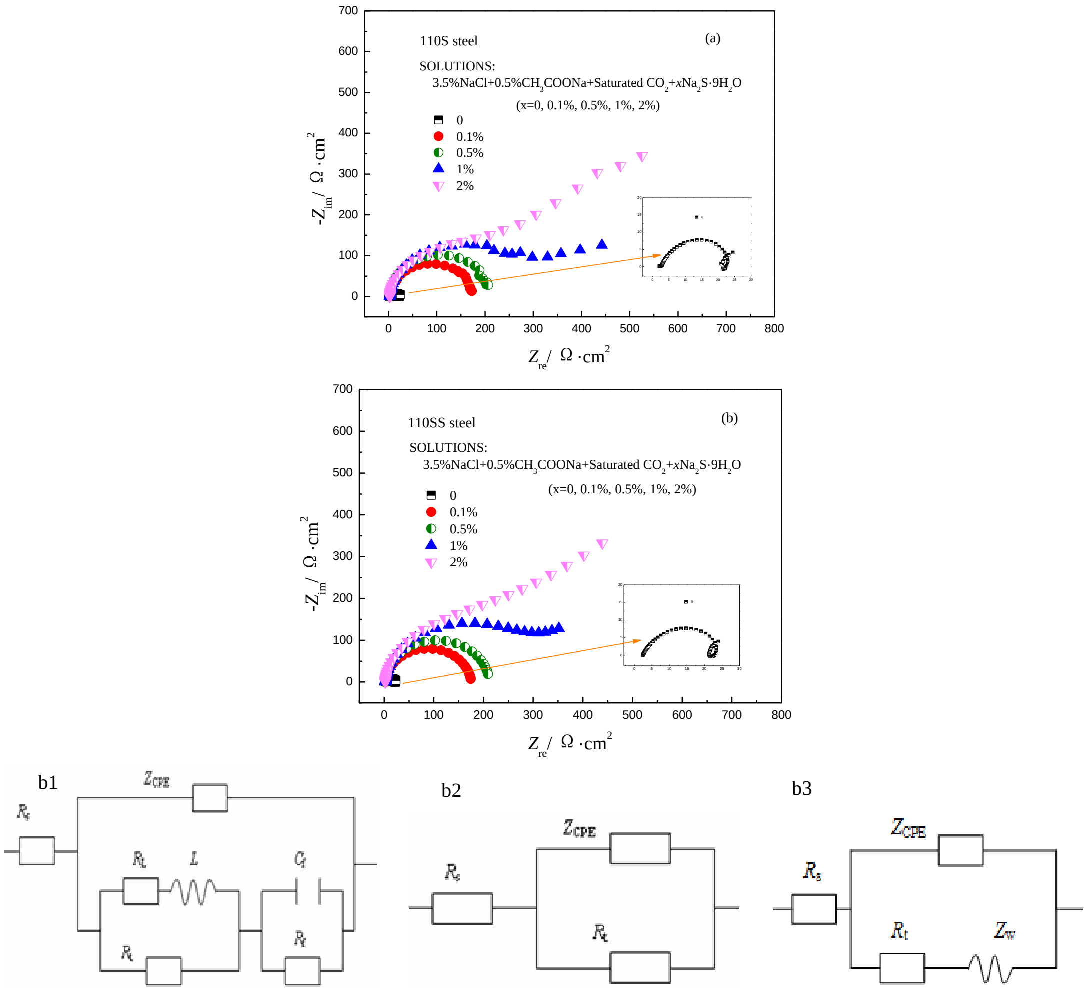

**Figure 5.** Effect of $H_2S$ on Nyquist plots of 110SS steel at 45°C in acidic solutions containing $H_2S$ and $CO_2$. (a) testing curves; (b) fitting curves and equivalent current models

For the addition of $Na_2S{\cdot}9H_2O$ (0.1*wt*.% to 2.0*wt*.%) the inductive reactance semicircle and capacitive semicircle at the low frequency region disappear due to the active areas or adsorbed areas of steel surface completely occupied by corrosion product layers, and they are substituted by a line with dip angle approximately 45°C for 1.0*wt*.% and 2.0*wt*.% $Na_2S{\cdot}9H_2O$ cases, which is Warburg resistance characteristics at low frequency region. The corresponding Bode plots of 110SS steel at 45°C are presented in Fig. 6. It can be seen that the maximum phase angle peak shifts to the left direction (low frequency direction) and rises towards -90° significantly as the increase of $Na_2S\cdot9H_2O$ concentration, which reflects that the $H_2S/HS^-$ species plays an important role in the formation of more protective corrosion product layers for the corrosion resistance on meal surface.

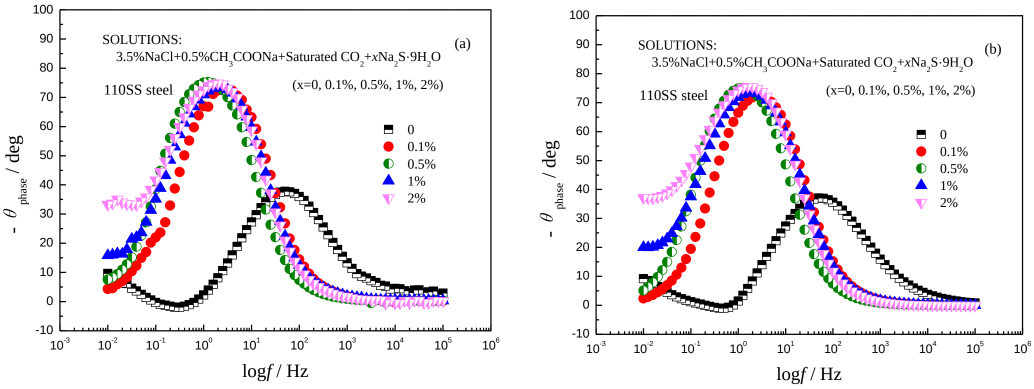

**Figure 6.** Effect of $H_2S$ on Bode plots of 110SS steel at 45°C in acidic solutions containing $H_2S$ and $CO_2$. (a) testing curves; (b) fitting curves

**Table 5.** Fitting parameters from the Nyquist plots of 110SS steel by equivalent circuit models at 45°C in acidic solutions containing $H_2S$ and $CO_2$

| Parameters | $x$ $Na_2S\cdot9H_2O$ | | | | |
|---|---|---|---|---|---|
| | 0 | 0.1% | 0.5% | 1% | 2% |
| $R_s$ ($\Omega\cdot cm^2$) | 2.4 | 2.4 | 2.3 | 2.6 | 2.4 |
| $Q$-$Y_0$ ($\Omega^{-1}\cdot cm^{-2}\cdot s^n$) | $2.3\times10^{-3}$ | $3.3\times10^{-3}$ | $6.4\times10^{-3}$ | $3.5\times10^{-3}$ | $3.9\times10^{-3}$ |
| $Q$-$n$ | 0.70 | 0.95 | 0.97 | 0.94 | 0.96 |
| $R_t$ ($\Omega\cdot cm^2$) | 25.2 | 172.9 | 209.7 | 277.1 | 223.3 |
| L ($H\cdot cm^2$) | 16.7 | - | - | - | - |
| $R_L$ ($\Omega\cdot cm^2$) | 79.6 | - | - | - | - |
| $C_f$ ($F\cdot cm^{-2}$) | 2.9 | - | - | - | - |
| $R_f$ ($\Omega\cdot cm^2$) | 8.4 | - | - | - | - |
| $Z_W$ ($\Omega\cdot cm^2$) | - | - | - | $2.3\times10^{-3}$ | $7.4\times10^{-4}$ |

According to the equivalent circuit models in Fig. 6, the corresponding fitting parameters from Nyquist plots obtained at 45°C by ZsimpWin software are listed in Table 5. It can be seen that in the presence of different amounts of $Na_2S\cdot9H_2O$, the $R_t$ values of 110SS steel have a greatly increase and larger than the one in $H_2S$-free solution except for 2.0*wt*.% $Na_2S\cdot9H_2O$. It indicates that $H_2S/HS^-$ can inhibits significantly corrosion attack to 110SS steel, which is in agreement with the results from the polarization curves at 45°C except for the 2.0*wt*.%.$Na_2S\cdot9H_2O$ case. The research result is in accordance with some researches [22]. The $R_t$ values of 110SS steel are respectively 277.1 $\Omega\cdot cm^2$ and 223.3 $\Omega\cdot cm^2$ in 1.0*wt*.% and 2.0*wt*.% $Na_2S\cdot9H_2O$ cases, which is probably caused by the larger diffusion resistance for the latter. In addition, it is also found that the corresponding $R_t$ value of 80S steel is smaller than that of 110SS steel at the same solution condition based on Table 4 and Table 5, indicating 110SS steel has better anti-sulfur performance than 80S steel in $H_2S$-containing environment. Another representative parameter in this work is the $Z_w$ value corresponding to species diffusion process. It is clear that the $Z_w$

value decreases with the increase of $Na_2S\cdot 9H_2O$ concentration from 1.0*wt*.% to 2.0*wt*.% at 45°C, so the corrosion resistance increases in the diffusion process. It can be explained by the fact that corrosion product layers formed on 110SS steel surfaces are relatively loose with the addition of 1.0*wt*.% $Na_2S\cdot 9H_2O$, the reaction ions can go through tiny holes in the product layers and gather in the activation region of naked substrate under the layers may lead to a low reactive resistance according to the research by Wang *et al.* [26]. As the addition of $Na_2S\cdot 9H_2O$ to 2.0*wt*.%, the more protective corrosion product layers will form and provide well better resistance to diffusion process, therefore the $Z_w$ value decreasing.

### *3.3. Analysis of corrosion product layers*

#### *3.3.1. Corrosion morphology*

Figure 7 illustrates the microscopic surface morphologies of corrosion product layers on 80S steel at 45°C in acidic solutions containing $H_2S$ and $CO_2$ for different concentrations of 0, 0.1*wt*.%, 0.5*wt*.%, 1.0*wt*.%, 2.0*wt*.% $Na_2S\cdot 9H_2O$. For the $H_2S$-free case, the corrosion product layers formed on 80S steel are squamaceous and loose, and peeled off at some positions such as $A_1$ as shown in Fig 7a. In the $H_2S$-containing environments, the microscopic characteristics of the "second deposition" crystals of corrosion products are distributed in the "first deposition" plat corrosion product layers on 80S steel surfaces and simultaneously there are large amounts of small cracks at some positions such as $B_1$, $C_1$ and $D_1$ as shown in Fig. 7b, Fig. 7c and Fig. 7d, which is attributed to an increasing internal stress in the dense corrosion product layer. At the regions where corrosion cracks formed, the corrosive species such as $Cl^-$, $H_2CO_{3(aq)}$, $HCO_3^-$ and $H_2S_{(aq)}$, $HS^-$ can readily pass through the cracked product layer and reach the layer/substrate interface, resulting in more serious localized corrosion. In addition, it can be observed in Fig. 7c that there exist some dark shadow areas left behind by the shedding of corrosion product grains, which demonstrates that the corrosion products have the low binding force with steel substrate metal. In Fig.7e, for high $H_2S$-containing environment (2.0*wt*.% $Na_2S\cdot 9H_2O$), the whole corrosion product layer is flat and dense, but localized corrosion occurs at many positions on coupon surface.

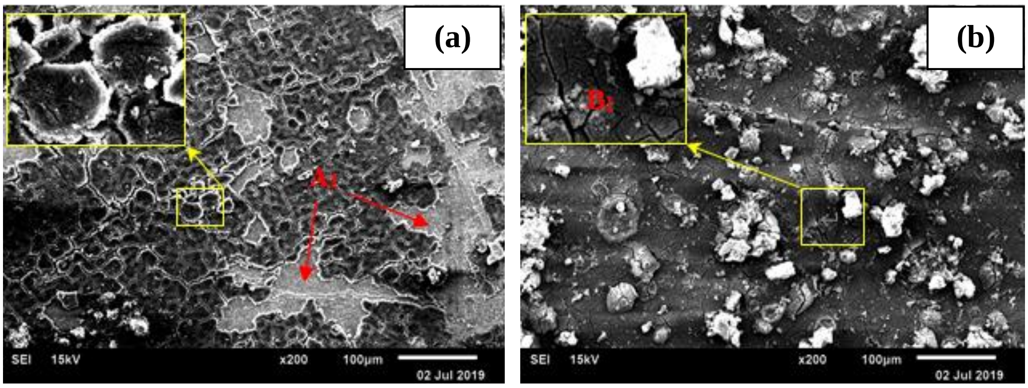

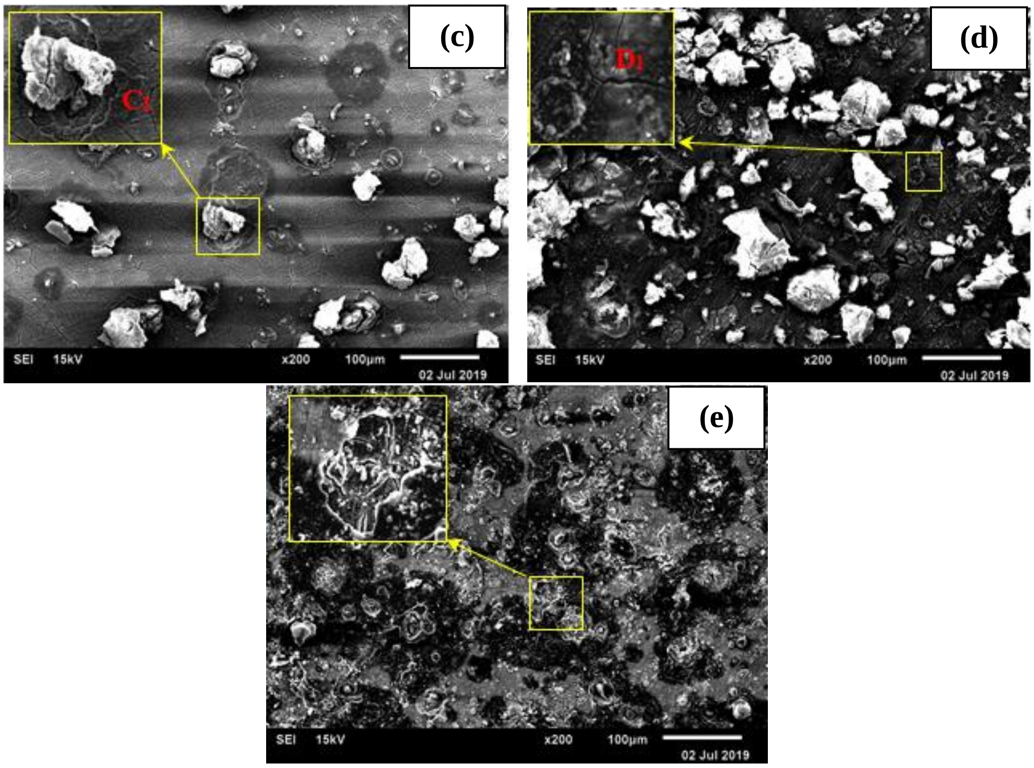

**Figure 7.** Surface morphologies of corrosion product layers on 80S steel at 45°C in acidic solutions containing $H_2S$ and $CO_2$ for different $Na_2S \cdot 9H_2O$ concentrations. (a) 0; (b) 0.1%; (c) 0.5%; (d) 1.0%; (e) 2.0%

Figure 8 also illustrates the microscopic surface morphologies of corrosion product layers on 110SS steel at same conditions. In Fig. 8a, the corrosion product layers are nor flat, liking ditch shape, and loose which can be observed from rectangular zoom zone. In the $H_2S$-containing solutions, it can be similarly seen that the “second deposition” crystals of corrosion products are distributed in the “first deposition” plat corrosion product layers on 110SS steel surfaces. Moreover, more amounts of “second deposition” crystals formed with the increase of $Na_2S \cdot 9H_2O$ concentration.

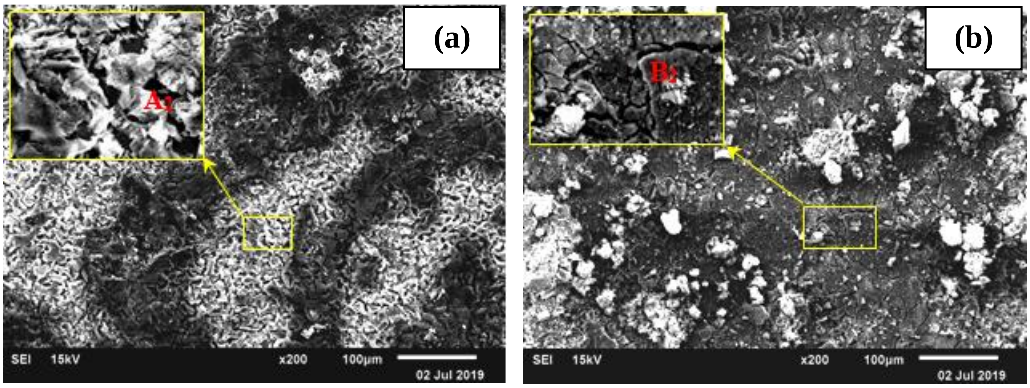

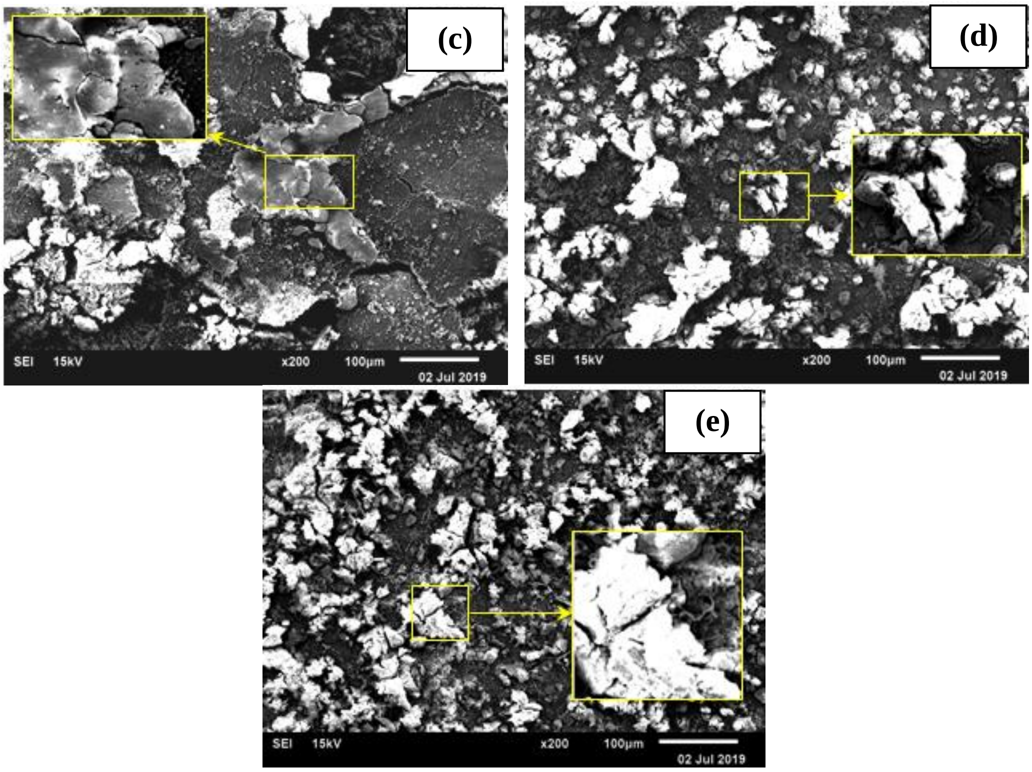

**Figure 8.** Surface morphologies of corrosion product layers on 110SS steel at 45ºC in acidic solutions containing $H_2S$ and $CO_2$ for different $Na_2S\cdot 9H_2O$ concentrations. (a) 0; (b) 0.1%; (c) 0.5%; (d) 1.0%; (e) 2.0%

In this proposed corrosion model as shown in Fig. 9, there are four stages related to the formation of corrosion product layers in in acidic solutions containing $H_2S$ and $CO_2$. First, the corrosive species such as $CO_{2(aq)}$, $H_2CO_3$, $HCO_3^-$, $CO_3^{2-}$ and $H_2S(aq)$, $HS^-$, $S^{2-}$ , $H^+$ are formed in the dissolved $H_2S/CO_2$ acid solution, and then these species can transfer towards the steel matrix surface to react with the released $Fe^{2+}$ ions, generating the thin and loose corrosion products related to sulfides such as $Fe_yS_x$, which is attributed to greatly small solubility product of iron sulfide contrast to iron carbonate. Second, in the static corrosion environment, the producing internal stress in corrosion product layer is not enough to the binding force between steel matrix and corrosion layer, and the corrosion product layer (iron sulfide) will thicken with testing time or more serious corrosion solutions. Third, there are some loose zones due to the existing individual defects in corrosion product layer, and the corrosive species can pass through the corrosion product layer and result in serious localized corrosion. And then it sequentially accelerates the pitting corrosion attributed to the effect of ‘big cathode and small anode’ in some individual sites. Fourth, when $H_2S$-related species diminish with $H_2S$ corrosion in the closed system, the $CO_2$-related species will react with the diffused iron ions away from steel matrix accompanying with $H_2S$ corrosion, so the corrosion product $FeCO_3$ will adsorb and precipitate on the corrosion product layer $Fe_yS_x$ formed early, resulting in thickening corrosion layers. Simultaneously, the localized corrosion pitting further extend, and probably the binding force between the metal matrix and the product layers weakens due to the effect of the producing stress. Ultimately, some individual corrosion pits can pierce the production pipeline due to the corrosion catalytic effect of closed-cell batteries.

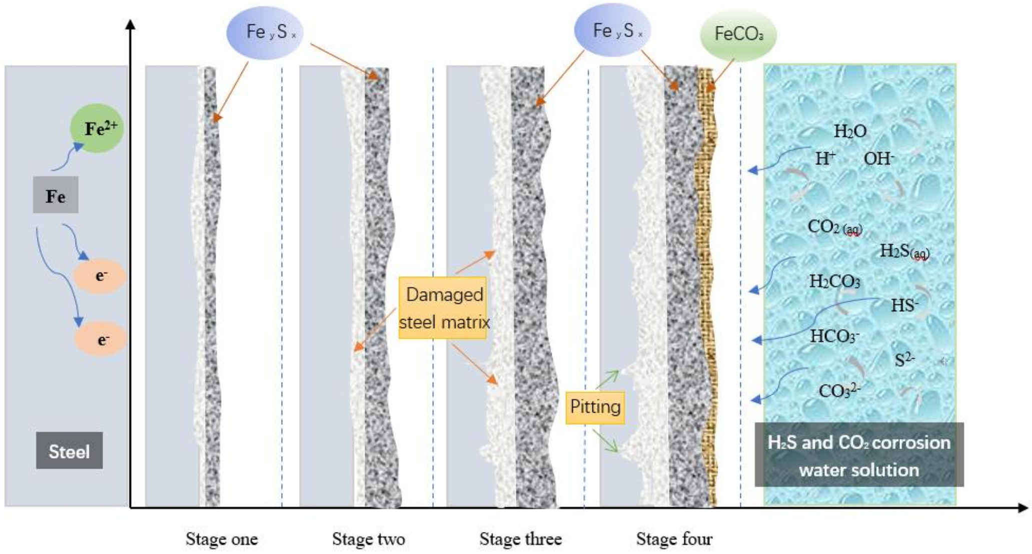

**Figure 9.** Schematic diagram of corrosion model for carbon steel in acidic solutions containing $H_2S$ and $CO_2$

### *3.3.2. EDX spectra*

The representative EDX spectra analysis of the corrosion products in 0.1*wt*.% and 1.0*wt*.% $Na_2S{\cdot}9H_2O$ cases at locations marked with arrows on SEM images of 80S and 110SS steels are shown in Fig. 10 and Fig. 11, respectively. The EDX analysis of each specimen is carried out at the accelerating voltage of 15 mV found to penetrate too deep into the substrate, therefore the element contents are not very accurate and only act as contrast and reference in various conditions.

In Fig. 10, the corrosion products of 80S steel mainly contain elements C, O, S and Fe, which are probably a mixture of iron carbonate, iron sulfides, and iron oxides due to the multiple reactants. For 0.1*wt*.% $Na_2S{\cdot}9H_2O$ case, the weak peak of Cr element is detected, but the small amount of C element is not revealed whereas the very weak C peak can be seen in Fig. 10a, inferring that $CO_{2(aq)}/HCO_3^-$ with respect to $H_2S_{(aq)}/HS^-$ have more lower active energy to react with steel. The iron sulphide of corrosion products is most likely mackinawite substance from previous studies [27]. It is worth noticing that the amounts of S element in the “first deposition” black corrosion product layer are higher than those in the “second deposition” gray corrosion product crystals (*i.e.*, 10.42*at*.% and 5.36*at*.% for 0.1*wt*.% $Na_2S{\cdot}9H_2O$, 12.54*at*.% and 9.91*at*.% for 1.0*wt*.% $Na_2S{\cdot}9H_2O$) as shown in Fig. 10a and 10b, which indicates that the black product layer contains more amounts of iron sulfides and that $H_2S$ corrosion preferentially happens related to $CO_2$ corrosion in mixed $H_2S/CO_2$ containing solution. In contrast to the 0.1*wt*.% $Na_2S{\cdot}9H_2O$ case, the amount of S element is lower than that for the 1.0*wt*.% $Na_2S{\cdot}9H_2O$ case.

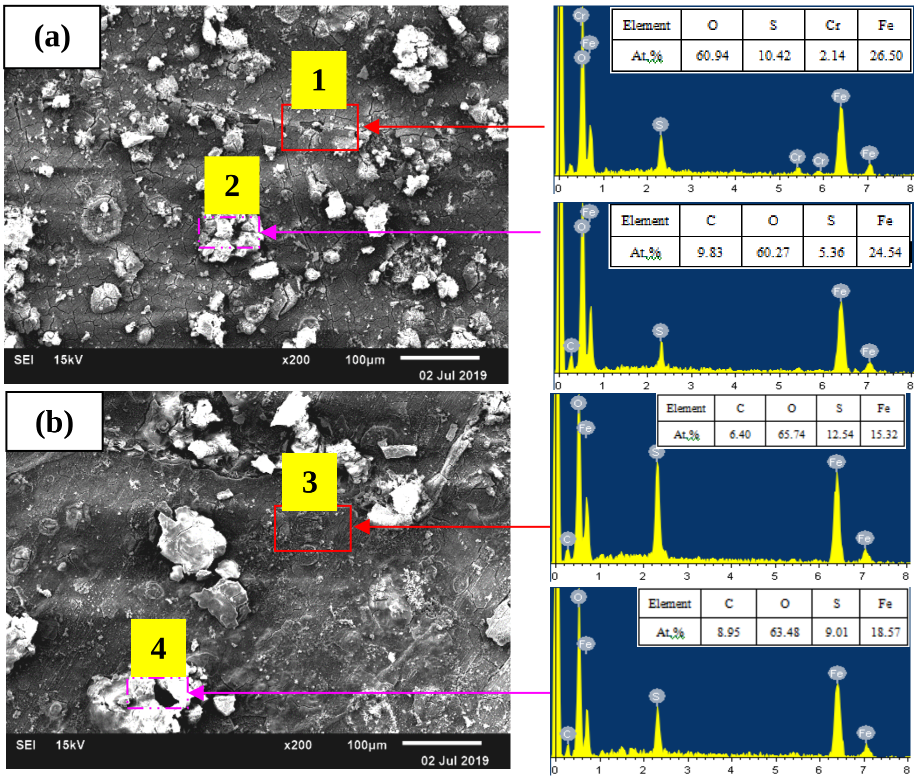

| Element | O | S | Cr | Fe |
|---|---|---|---|---|
| At.% | 60.94 | 10.42 | 2.14 | 26.50 |

| Element | C | O | S | Fe |
|---|---|---|---|---|
| At.% | 9.83 | 60.27 | 5.36 | 24.54 |

| Element | C | O | S | Fe |
|---|---|---|---|---|
| At.% | 6.40 | 65.74 | 12.54 | 15.32 |

| Element | C | O | S | Fe |
|---|---|---|---|---|
| At.% | 8.95 | 63.48 | 9.01 | 18.57 |

**Figure 10.** EDX analysis of corrosion product layers on 80S steel at 45°C in acidic solutions containing $H_2S$ and $CO_2$. (a) 0.1% $Na_2S\cdot 9H_2O$; (b) 1% $Na_2S\cdot 9H_2O$

In Fig. 11, the similar characteristics of the amount of S element in corrosion products of 110SS steel can be seen as that of 80S steel. The S element of “first deposition” and “second deposition” corrosion product layers are 8.40*at*.%, 4.76*at*.% for 0.1*wt*.% $Na_2S\cdot 9H_2O$ and 12.27*at*.%, 2.80*at*.% for 1.0*wt*.% $Na_2S\cdot 9H_2O$, respectively. Considering $OH^-$, $CH_3COO^-$, $H_2CO_{3(aq)}$, $HCO_3^-$, $H_2S_{(aq)}$ and $HS^-$ as the main reactants for anodic reactions, the competition of the surface coverage is influenced by the concentration and the nature of each ion like the structure and the specific adsorption. $CH_3COO^-$, $H_2CO_{3(aq)}$ and $HCO_3^-$ ions have a larger size, so $OH^-$, $H_2S_{(aq)}$ and $HS^-$ can more easily occupy the inner Helmholtz plane on the steel surface and can be likely to form the inner layer (*i.e.*, “first deposition” layer).

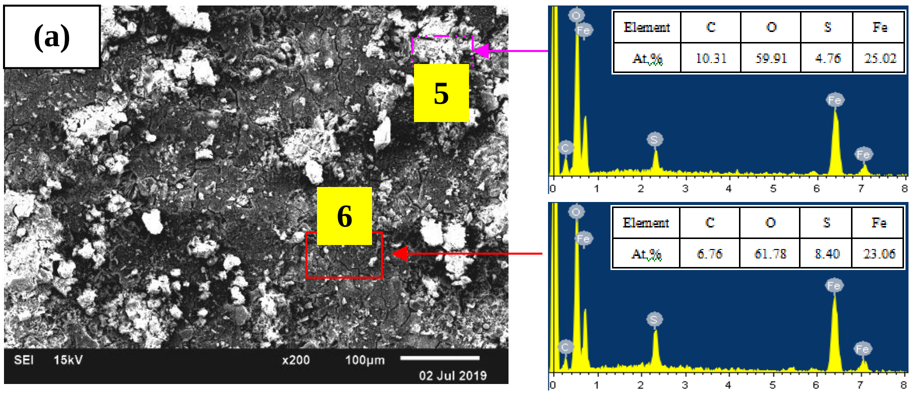

| Element | C | O | S | Fe |
|---|---|---|---|---|
| At.% | 10.31 | 59.91 | 4.76 | 25.02 |

| Element | C | O | S | Fe |
|---|---|---|---|---|
| At.% | 6.76 | 61.78 | 8.40 | 23.06 |

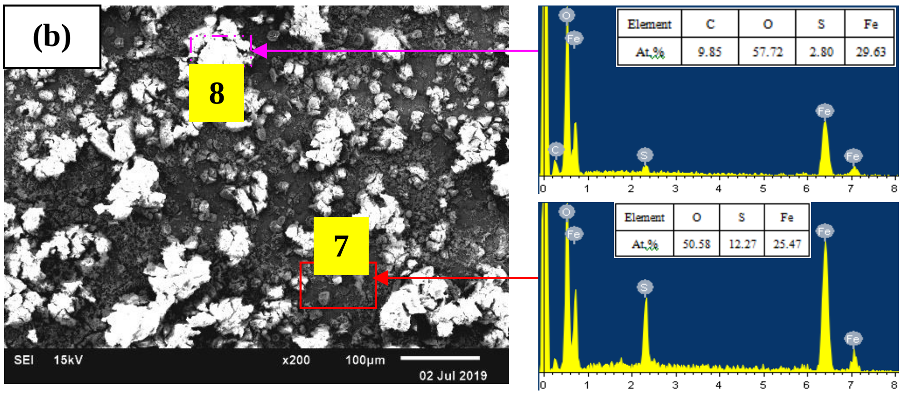

| Element | C | O | S | Fe |
|---|---|---|---|---|
| At.% | 9.85 | 57.72 | 2.80 | 29.63 |

| Element | O | S | Fe |
|---|---|---|---|
| At.% | 50.58 | 12.27 | 25.47 |

**Figure 11.** EDX analysis of corrosion product layers on 110SS steel at 45ºC in acidic solutions containing $H_2S$ and $CO_2$. (a) 0.1% $Na_2S\cdot 9H_2O$; (b) 1% $Na_2S\cdot 9H_2O$

According to the previous researches [28], the various polymorphs of iron sulfide can form as corrosion products in $H_2S$-containing corrosion of mild steel, including amorphous ferrous sulfide (FeS), mackinawite (FeS), cubic ferrous sulfide (FeS), troilite (FeS), pyrrhotites ($Fe_{1-x}S$), smythite ($Fe_{3+x}S_4$), greigite ($Fe_3S_4$), pyrite ($FeS_2$) and marcasite ($FeS_2$). Mackinawite is a tetragonal sulfur-deficient iron sulfide with a composition of either $FeS_{1-x}$ (x=0~0.07) or $Fe_{1+x}S$ (x=0.057~0.064), which is considered unstable and a main corrosion product on carbon steel surface. Pyrrhotite is more stable than mackinawite and it is iron-deficient iron sulfide with a composition ranging from $Fe_7S_8$ to stoichimetric troilite FeS. Moreover, trolilite appears as a kind of corrosion product in aqueous $H_2S$-containing at low temperatures due to high local iron concentrations at the corroding surface.

In this work, the result from EDX spectra shows that the corrosion products contain most common siderite ($FeCO_3$) and most probably polymorphs of iron sulfide such as mackinawite (FeS) or pyrrhotites ($Fe_{1-x}S$) based on the Fe:S ratios and that the C:O ratios as the change of $Na_2S\cdot 9H_2O$ concentration.

## 4. CONCLUSIONS

The cathodic branch curve shifts to the current decreasing direction with the increase of $Na_2S\cdot 9H_2O$ (*i.e.*, $H_2S/HS^-$) concentration. Corrosion potential ($E_{corr}$) becomes more negative and corrosion current density ($i_{corr}$) decreases with increasing $Na_2S\cdot 9H_2O$ concentration. As compared to the $i_{corr}$ values of 80S steel, the corresponding $i_{corr}$ value of 110SS steel decreases at same solution condition indicating that 110SS steel has stronger resistance than 80S steel in the $H_2S$ containing environment.

The small depressed capacitive semicircle and inductive reactance semicircles in the low frequency region disappear with the addition of $Na_2S\cdot 9H_2O$. For 1.0*wt*.% and 2.0*wt*.% $Na_2S\cdot 9H_2O$ cases, Warburg impedance characteristics of diffusion process on 110SS steel in low frequency region is observed following a depressed capacitive semicircle in the intermediate frequency region. The phase angle peaks for $H_2S$ containing cases at intermediate frequency shift to a lower frequency and raises toward -90° significantly. In the presence of different amounts of $Na_2S\cdot 9H_2O$, the $R_t$ value has a significant increase and the $Z_w$ value decreases with $Na_2S\cdot 9H_2O$ concentration increasing.

The Microscopic "second deposition" crystals of corrosion products are distributed in the "first deposition" plat corrosion product layers on steel surfaces, and amounts of corrosion cracks formed in localized zones. The corrosion products mainly contain elements C, O, S and Fe, which are probably a mixture of iron carbonate, iron sulfides, and iron oxides. The amount of S element in the "first deposition" corrosion product layer is higher than that in the "second deposition" corrosion product crystals.

ACKNOLEDGMENTS
The authors kindly thank the support to this work for experimental setup supplied by Shaanxi Yanchang Petroleum (Group) Co. LTD, and the financial support from Xi'An Science and Technology Planning Project (2017CGWL09).

## References

1. F.X. Shi, L. Zhang, J.W. Yang, M.X. Lu, J.H. Ding, and H. Li, *Corros. Sci.*, 102 (2016) 103.
2. M.A. Mohtadi-Bonab, M. Eskandari, K.M.M. Rahman, and R. Ouellet, Int. *J. Hydrogen. Energ.*, 41 (2016) 4185.
3. D.P. Li, L. Zhang, J.W. Yang, and M.X. Lu, *Int. J. Min. Met. Mater.*, 21 (2014) 388.
4. J. Bana's, U. Lelek-Borkowska, B. Mazurkiewicz, and W. Solarski, *Electrochim. Acta*, 52 (2007) 5704.
5. L. Wei, X.L. Pang, and K.W. Gao, *Corros. Sci.*, 103 (2016) 132.
6. R. Galvan-Martinez, J. Mendoza-Flores, R. Duran-Romero, and J. Genesca-Llongueras, *Mater. Corros.*, 55 (2004) 586.
7. J. Kittel, F. Ropital, F. Grosjean, E.M.M. Sutter, and B. Tribollet, *Corros. Sci.*, 66 (2013) 324.
8. A. Kahyarian, and S. Nesic, *Electrochim. Acta*, 297 (2019) 676.
9. C. Sun, J. Sun, Y. Wang, X. Lin, X. Li, X. Chen, and H. Liu, *Corros. Sci.*, 107 (2016) 193–203.
10. Z.Q. Bai, Z.F. Yin, D. Wei, X.F. Wang, and C.X. Yin, *Mater. Corros.*, 61 (2010) 689.
11. X.L. Cheng, H.Y. Ma, J.P. Zhang, X. Chen, S. H. Chen, and H. Q. Yang, *Corrosion*, 54 (1998) 369.
12. H.Y. Ma, X.L. Cheng, G.Q. Li, S.H. Chen, Z.L. Quan, S.Y. Zhao, and L. Niu, *Corrosion*, 54 (1998) 634.
13. K. Masamura, S. Hashizume, and J. Sakai, *Corrosion*, 6 (1987) 359.
14. M.E. Orazem, and B. Tribollet, Electrochemical impedance spectroscopy, *Wiley ed.*, in: The Electrochemical Society Series (second ed.), 2017.
15. S. Arzola, and J. Genesca, *J. Solid State Electrochem.*, 9 (2005) 197.
16. Standard Technical Method, NACE TM 01 77, *NACE*, 1996.
17. J.L. Crolet, N. Thevenot, and S. Nesic, *Corrosion*, 54 (1998) 194.
18. M.M. Singh, and A. Gupta, *Corrosion*, 56 (2000) 371.
19. Y. Choi, S. Nesic, and S. Ling, *Electrochim. Acta*, 56 (2011) 1752.
20. M.A. Veloz, and I. Gonzalez, *Electrochimica Acta*, 48 (2002) 135_/144
21. J. Tang, Y. Shao, J. Guo, T. Zhang, G. Meng, and F. Wang, *Corros. Sci.*, 52 (2010) 2050.
22. H.Y. Ma, X.L. Cheng, G.Q. Li, S.H. Chen, Z.L. Quan, S.Y. Zhao, and L. Niu, *Corros. Sci.*, 42 (2000) 1669.
23. E. McCafferty, *Corros. Sci.*, 39 (1997) 243.
24. D.C. Silverman, and J.E. Carrico, *Corrosion*, 44 (1988) 280.
25. S. Walkner, and A.W. Hassel, *Electrochim. Acta*, 131 (2014) 130.
26. B. Wang, C. Cui, and S. Zhang, *Mater. Chem. Phys.*, 198 (2017) 7.
27. F.W. Song, *Electrochim. Acta*, 55 (2010) 689.

28. W. Sun, S. Nesic, and D. Young, *Ind. Eng. Chem. Res.*, 47 (2008) 1738.